ORIGINAL ARTICLE

A model for transcutaneous current stimulation: simulations and experiments

Andreas Kuhn · Thierry Keller · Marc Lawrence · Manfred Morari

Abstract Complex nerve models have been developed for describing the generation of action potentials in humans. Such nerve models have primarily been used to model implantable electrical stimulation systems, where the stimulation electrodes are close to the nerve (near-field). To address if these nerve models can also be used to model transcutaneous electrical stimulation (TES) (far-field), we have developed a TES model that comprises a volume conductor and different previously published non-linear nerve models. The volume conductor models the resistive and capacitive properties of electrodes, electrode-skin interface, skin, fat, muscle, and bone. The non-linear nerve models were used to conclude from the potential field within the volume conductor on nerve activation. A comparison of simulated and experimentally measured chronaxie values (a measure for the excitability of nerves) and muscle twitch forces on human volunteers allowed us to conclude that some of the published nerve models can be used in TES models. The presented TES model provides a first step to more extensive model implementations for TES in which e.g., multi-array electrode configurations can be tested.

Keywords Transcutaneous electrical stimulation · Finite element model · Active nerve model · Capacitive effects

A. Kuhn (✉) · T. Keller · M. Lawrence · M. Morari
Automatic Control Laboratory, ETH Zurich,
Physikstrasse 3, 8092 Zurich, Switzerland
e-mail: kuhnan@control.ee.ethz.ch

A. Kuhn · M. Lawrence
Sensory-Motor Systems Laboratory,
ETH Zurich, 8092 Zurich, Switzerland

T. Keller
Biorobotics Department, Fatronik-Tecnalia,
2009 Donostia-San Sebastian, Spain

Abbreviations

TES	Transcutaneous electrical stimulation
AP	Action potential
PD	Pulse duration
FE	Finite element
TP	Transmembrane potential
$V_{FE}(t)$	Electric scalar potential
σ	Conductivity
ρ	Resistivity
ε_r	Permittivity
$V_n(t)$	Transmembrane potential at node n and time t
$V_{e,n}(t)$	Extracellular potential at node n and time t
$I_{i,n}(t)$	Ionic current at node n and time t
C_m	Membrane capacitance
G_a	Conductance of the axoplasm
I_{rh}	Rheobase
T_{ch}	Chronaxie
I_{th}	Threshold current
τ_{sim}	Time constant of simulated recruitment-duration curve
τ_{exp}	Time constant of measured recruitment-duration curve
Rec	Recruitment
Rec_{sat}	Saturation value of recruitment
g_L	Nodal leakage conductance
ϱ_i	Axoplasmatic resistivity

1 Introduction

Transcutaneous electrical stimulation (TES) can be used to artificially activate nerve and muscle fibers by applying electrical current pulses between pairs of electrodes placed on the skin surface. The applied current flows through the skin and underlying tissues (bulk tissues) where a spatio-temporal potential field is generated depending on the resistivities and permittivities (capacitance) of the various tissues. Axons distributed in nerve bundles that lie within the bulk tissues experience activation and can generate action potentials (APs) due to the electrically induced potential field. These APs travel along the axons to the muscle where a contraction of the muscle is generated. For single stimulation pulses the generated twitch force is increased when the pulse amplitude or the pulse duration (PD) is increased [2] because additional axons are recruited in the nerve bundles [45].

Two-step models have been proposed to describe nerve activation in TES [38]. The first step describes the electrical potential field within the electrodes, the electrode-skin interfaces, and the bulk tissues (volume conductor). Analytical models [32, 39] finite difference models [34], and finite element (FE) models [35] were used to calculate the potential field in the volume conductor. The second step describes the complex behavior of the axons' transmembrane potential (TP), which depends upon the spatiotemporal potential field along the axon [37]. Several two step models were proposed to describe TES [27, 43, 51]. However, these models exclusively employ static models (i.e. neglecting capacitive effects) to describe the volume conductor, and linear nerve models to describe nerve activation. Up to now non-linear nerve models, which can describe more facets of nerve activation [45], were mainly used for implantable systems [31, 49, 47], epidural stimulation [18], or motor cortex stimulation [33], where the exciting electrodes are small and close to the nerve (near-field). To address if these nerve models can also be used to model TES (far-field), we have developed a TES model that comprises a volume conductor and different non-linear nerve models. Such a model that describes TES from the applied stimulation current pulse to nerve recruitment is useful for the development and enhancement of new stimulation technology. For example, the irregular potential fields that are delivered with multi-channel array electrodes [8, 30] can be described using such models. These irregular potential fields produced with multi-channel array electrodes can be varied spatially and temporally and require time varying solutions to describe nerve activation appropriately. In this paper a suitable axon model to be used in such a TES model is identified and verified with experiments.

A method to experimentally verify electrical stimulation models is to compare simulated strength-duration curves with experimentally obtained strength-duration data [52]. Strength-duration curves describe the stimulation current amplitude versus the PD for threshold activation. From strength-duration curves rheobase and chronaxie can be derived [13]. The rheobase is the smallest current amplitude of 'infinite' duration (practically, a few hundred milliseconds) that produces an activation. Chronaxie is the PD required for activation with an amplitude of two times the rheobase. Experimentally obtained chronaxie values using electrodes placed close to the excited axon (clamp experiments, animal studies and needle electrodes) are between 30 and 150 μs [3, 9, 42]. Published non-linear nerve models were experimentally verified in this range of chronaxie values [4, 37, 38, 42, 52]. However, chronaxie values that were obtained experimentally using surface electrodes are longer. In humans the chronaxie values using surface electrodes were found to be between 200 and 700 μs [15, 23, 48]. It is unclear if the short chronaxie values (30–150 μs) of such non-linear nerve models that were designed for implantable systems are increased significantly when used in a TES model to describe chronaxie values measured with surface electrodes in TES (200–700 μs).

Apart from strength-duration curves, which describe only the excitability at motor threshold (thickest axons activated), measured force or torque versus PD curves were used to describe the excitability of nerves (where also thinner axons are activated) [45]. Such measurements at higher stimulation intensities provide additionally an understanding of the nerve recruitment. These curves show either the stimulation amplitude versus the PD at a fixed force output [6, 22, 54] or the force versus the PD at a fixed amplitude [1, 14]. The influence of the muscle properties on the measurement can be minimized by measuring twitch forces (single stimulation pulse) instead of tetanic forces [2]. This has the advantage that experimentally measured twitch forces can be directly compared with nerve recruitment obtained from nerve models [31]. As such, we present twitch force measurements on human volunteers that are compared with the nerve recruitment from our TES model. This comparison enabled us to conclude, which nerve models are most suitable to be used in TES models.

2 Methods

2.1 TES model

The developed TES model comprises an FE model that describes the potential field in the volume conductor
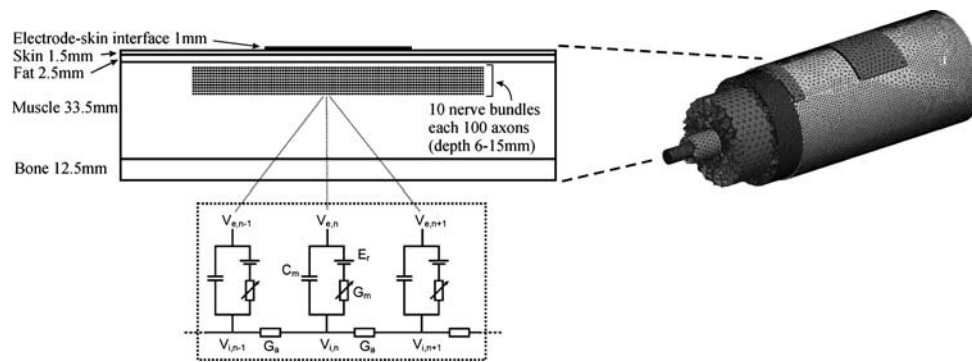
Fig. 1 Schematic representation of the electrode-skin interface, the bulk tissues, and ten nerve bundles at depths between 0.6 and 1.5 cm (from skin surface). On the bottom the electrical equivalent circuit of a myelinated axon. On the right the meshed geometry of the arm model with surface electrodes (some tissue layers are partially removed for clarity). The model comprised approximately 300,000 tetrahedral elements

(forearm) and an active (non-linear) nerve model that calculates nerve activation. The following two subsections introduce the two models and how they are linked together.

2.1.1 Finite element model

The electric scalar potential (V_{FE}) within the arm model (volume conductor) and the electrodes was described by Eq. 1, which can be derived from Amperes's Law. It takes into account both the resistive (σ) and the dielectric properties ($\varepsilon = \varepsilon_0 \varepsilon_r$) of the tissues. The electrical potentials were calculated with the finite element time domain (FETD) solver of the FEM package Ansys (EMAG, Ansys Inc., Canonsburg, PA).

$$-\nabla \cdot ([\sigma]\nabla V_{FE}) - \nabla\left([\varepsilon]\nabla\frac{\partial V_{FE}}{\partial t}\right) = 0 \qquad (1)$$

The two stimulation electrodes were modeled as a good conducting substrate (conductive carbon rubber) with a 1 mm thick electrode-skin interface layer (hydrogel) with a size of 5 cm by 5 cm and a center to center spacing of 11 cm. These parameters were chosen as in the experimental setup (Sect. 2.2). The amplitudes and durations of the current-regulated pulses that were applied to the electrodes could be varied. The bulk tissues were modeled with a multiple layer cylinder (Fig. 1) representing the forearm. A comparison of a cylindrical model geometry with a more detailed geometry segmented from MRI scans, revealed that nerve activation did not change significantly (<5%) using the more detailed geometry [26]. Therefore, a cylindrical geometry was used comprising skin, fat, muscle and bone layers with the thicknesses of 1.5 mm (skin), 2.5 mm (fat), 33.5 mm (muscle), 6 mm (cortical bone) and 6.5 mm (bone marrow). The cylinder had a length of 40 cm. The FE model was verified in [24] with experimental measurements where the potential on the skin and the potential in the muscle were measured and compared.

Table 1 Resistivities and relative permittivities of different tissues

		Min	Standard	Max
Electrode interface	$\rho[\Omega m]$		300	
	ε_r	1	1	2,000,000
Skin	$\rho[\Omega m]$	500	700	6,000
	ε_r	1,000	6,000	30,000
Fat	$\rho[\Omega m]$	10	33	600
	ε_r	1,500	25,000	50,000
Muscle (axial)	$\rho[\Omega m]$	2	3	5
	ε_r	100,000	120,000	2,500,000
Muscle (radial)	$\rho[\Omega m]$	6	9	15
	ε_r	33,000	40,000	830,000
Cortical bone	$\rho[\Omega m]$	40	50	60
	ε_r		3,000	
Bone Marrow	$\rho[\Omega m]$	10	12.5	15
	ε_r		10,000	

The column "Standard" contains properties used in an FE model that was verified with experimental measurements [24]

Columns "Min" and "Max" are extreme values from [10, 12, 40, 45]

The electrical properties (resistive and capacitive) that were used for the tissues and electrodes are given in Table 1. The anisotropy of the muscles' resistivity and permittivity was considered using a factor of three (between axial and radial direction $3*\rho_{axial} = \rho_{radial}$) [45].

The resulting time dependent potential field of the FE model was interpolated onto lines at different depths, which represented nerve bundle locations that were parallel to the longitudinal axis of the arm model. The potential at time t and position n on one nerve line is labelled $V_{FE,n}(t)$.

2.1.2 Nerve models

Four different active axon models (see Table 2) were combined with the FE model. These myelinated axon models were chosen to cover different axon model

Table 2 Comparison of published chronaxie values with chronaxie values obtained with the TES model (static volume conductor). Further, the rheobasic currents of the TES model for the different nerve models are given

Nerve model ID	Axon model name	Published chronaxie values (μs)	Chronaxie in TES model (μs)	Rheobase in TES model (mA)
A	Active cable model (FH) [38]	100	157	29.3
B	Active cable temperature Comp. (FH) [42, p.86]	100	137	29.2
C	Active mammalian nerve (CRRSS) [4, 52]	26	33	35.1
D	Active double cable (MRG model) [37]	150	457	2.97

structures and a wide range of chronaxie values (near-field) [55] (published chronaxie values are given in Table 2). Models A and B are based on the Frankenhaeuser-Huxley membrane [11] that describe sodium, potassium, and leakage membrane currents [38] of the nodes of Ranvier. Model C is the CRRSS model (CRRSS stands for its authors' names) that only incorporates sodium and leakage currents at the nodes of Ranvier. The CRRSS membrane is similar to the Hudgkin-Huxley membrane [17] but without potassium channels because they were found to be less important in the excitation process of myelinated mammalian nerves [52]. Model D (MRG model) incorporates a double cable structure that does not only describe membrane currents at the nodes of Ranvier but also at the paranodal and internodal sections [37].

The four introduced axon models describe the TP of a single axon with a certain diameter. However, in humans axons are gathered in nerve bundles consisting of many axons with different diameters. Multiple nerve bundles innervate muscles and these nerve bundles lie in different depth within the body [50]. Therefore, the four axon models (Table 2) were joined to multiple nerve bundles that lie in different depths underneath the stimulating electrode. The nerve bundles had a length of 15 cm and were centered under the cathode at depths (from skin) between 0.6 cm and 1.5 cm with 0.1 cm spacing (see Fig. 1). Each of the ten nerve bundles consisted of 100 axons with diameters distributed according to the bimodal distribution in human nerve bundles with peaks at 6 and 13 μm [41, 46]. The minimal axon diameter was 4 μm and the maximal diameter was 16 μm. Recruitment (Rec) was defined as the percentage of axons that were activated in all nerve bundles that consisted in total of 1,000 axons (10 nerve bundles each 100 axons). Axons with different diameters had different internodal distances ranging from 0.4 to 1.6 mm. The first nodes of all axons in each nerve bundle were aligned with each other. Initial fiber activation was verified in order to make sure that the AP was not initiated at the nerve model boundary. The threshold of the TP to detect activation was set to 0 mV. Additionally, only axons with propagating APs were counted as activated by ensuring that after detection of the initial AP also at all other nodes the TP was above 0 mV.

Nerve models A, B and C (Table 2) were implemented in MATLAB (The Mathworks Inc., Natick, MA) and Model D in NEURON [16]. Parameters in all nerve models were used as published (references are given in Table 2). The underlying equation of nerve models A to C is given in (2). $V_n(t)$ is the TP at node n (nodes of Ranvier) and time t, $V_{e,n}(t)$ is the extracellular potential, $I_{i,n}(t)$ is the ionic current, C_m is the membrane capacitance, and G_a is the conductance of the axoplasm (equivalent circuit given on the bottom of Fig. 1). Nerve model D (MRG) has a more complex structure and also takes into account the extracellular potentials at non-nodal compartments between the nodes of Ranvier $V_{e,n-n}(t)$.

$$\frac{dV_n(t)}{dt} = \frac{1}{C_m}[G_a(V_{n-1}(t) - 2V_n(t) + V_{n+1}(t) + V_{e,n-1}(t) - 2V_{e,n}(t) + V_{e,n+1}(t)) - I_{i,n}(t)] \quad (2)$$

The link between the FE model and the nerve models was established by assigning the time dependent, spatially interpolated potentials from the FE model $V_{FE,n}(t)$ to the corresponding extracellular potentials of the nerve model $V_{e,n}(t) = V_{FE,n}(t)$. When using nerve model D additionally the non-nodal extracellular potentials were interpolated in the FE model and assigned to the axon models $V_{e,n-n}(t) = V_{FE,n-n}(t)$.

2.2 Experimental measurements

Experimental measurements were performed on three human volunteers (age: 25–28, one female, two male) in order to verify the TES model. Two main aspects of the TES model were verified with two sets of experiments: motor thresholds were measured in order to compare strength-duration curves (Sect. 3.4), and isometric twitch forces were measured in order to compare recruitment-duration curves (Sect. 3.5) with results of the TES model.

In all experiments rectangular, monophasic current regulated pulses were applied with a Compex Motion Stimulator [21]. The motor point of the Flexor Digitorum Superficialis that articulates the middle finger was identified with a stainless steel probe with 0.5 cm tip diameter. The probe was moved over the muscles until the point that required the least current to generate minimal movement of
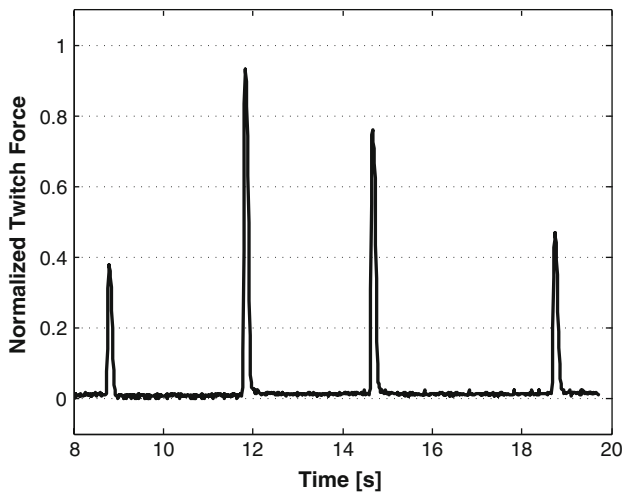
Fig. 2 Extract of the raw twitch force data of the middle finger that was measured with the DGAS measurements system. Single stimulation pulses with different PDs were randomly applied every 2.5–5 s

the middle finger was identified. Because surface motor points move depending on the configuration of the arm, the arm was set up in the isometric condition that was used during the force measurements. Following the identification of the motor point, the active electrode (cathode) (5 cm by 5 cm, hydrogel) was placed centered over the identified motor point and the indifferent electrode (anode) was placed at the wrist. In order to avert potentiation 300 stimulation pulses were applied prior to data capture.

The motor thresholds were determined by palpation of the region over the muscle. We stimulated with single pulses of 0.05, 0.1, 0.3, 0.5, 0.7, 1, and 2 ms duration. The amplitude of the stimulation pulse was increased in 0.3 mA steps for each PD until motor activation was felt by the examiner. The resting periods between applying the different pulse durations were 20 s.

After a resting period of 1 min the isometric twitch forces of the middle finger were measured with the dynamic grasp assessment system (DGAS) [20]. Single stimulation pulses with an amplitude of 20 mA and with PDs of 0.05, 0.1, 0.3, 0.5, 0.7, 1, and 2 ms were randomly applied every 2.5–5 s. Each PD was applied a total of six times (randomized). An extract of the raw twitch force measurements is shown in Fig. 2. Each data series was normalized to its maximal value in order to obtain recruitment-duration curves.

2.3 Strength-duration curves, rheobase, and chronaxie

Rheobase I_{rh} and chronaxie T_{ch} from strength-duration curves calculated with the TES model were compared with own experimentally obtained and previously published experimental rheobase and chronaxie values. In the TES model strength-duration curves were obtained by

calculating threshold currents I_{th} for PDs of 0.05, 0.1, 0.3, 0.5, 0.7, 1, and 2 ms. The threshold amplitudes were determined using bisection search with an accuracy of 0.01 mA. At threshold only the thickest axon model closest to the electrode was activated (axon diameter: 16 μm, depth: 0.6 cm). In the experiments motor thresholds were measured as described in Sect. 2.2. Lapicque's equation $I_{th} = I_{rh}/(1-\exp(-PD/T_{ch}))$ [29] was fit to the measured strength-duration data in order to obtain I_{rh} and T_{ch}. R-square (R^2) values between the fitted curves and the actual strength-duration data were calculated to check the accuracy of the fit (all values were below 0.8%).

2.4 Influence of tissue and stimulation parameters on chronaxie

The influence of tissue properties on the chronaxie was investigated in order to find out how the chronaxie changes for different tissue thicknesses, tissue properties, electrode sizes, and nerve depths. The aim was to investigate by computer modeling which parameters cause the large range of chronaxie values (200–700 μs) observed in strength-duration measurements with surface electrodes (far-field situation).

Tissue thicknesses of the forearm model were changed in the range of values that cover most human forearms [45, 50, 53]. The range of thicknesses was: for skin from 1 to 3 mm, fat from 2 to 30 mm, muscle from 20 to 60 mm, cortical bone from 4 to 8 mm, and bone marrow from 4 to 8 mm. The range of resistivity values that were tested are summarized in Table 1 (columns Min and Max) and cover the range of values that can be expected in practical applications of TES [10, 12, 40, 45]. Electrode size was kept at 5 cm × 5 cm when changing tissue thicknesses and tissue properties. Afterwards, chronaxie values for electrode sizes between 0.1 cm × 0.1 cm and 7 cm × 7 cm and two nerve depths of 0.6 and 1.5 cm were calculated. Electrode sizes below 0.5 cm × 0.5 cm are usually not used in TES and were included to allow a comparison of our simulated chronaxie values with publications that use point sources as electrodes. The changes in chronaxie values were calculated for all four nerve models (A to D).

2.5 Recruitment-duration curves and time constants

Simulated recruitment-duration curves were compared with experimentally obtained recruitment curves by comparing the corresponding time constants τ [5]. The time constants τ_{sim} of the recruitment-duration curves from the TES model were compared with the time constants τ_{exp} of the experimentally measured recruitment-duration curves (twitch forces). Both time constants were calculated by fitting Eq. 3 to the recruitment data as suggested in [5].

$$\text{Rec} = \text{Rec}_{\text{sat}}(1 - e^{-(\text{PD}-\text{PD}_0)/\tau}) \quad \text{for PD} \geq \text{PD}_0 \tag{3}$$

$$\text{Rec} = 0 \quad \text{for PD} < \text{PD}_0 \tag{4}$$

Rec is the recruitment, Rec_{sat} is the value where the recruitment saturates, PD represents the stimulation PD, PD_0 is the threshold PD above which an AP is generated, and τ is the time constant of the rising recruitment. R-square (R^2) values between the fitted curves and the actual recruitment data were calculated to check the accuracy of the fit (all values were below 1.5%).

3 Results

3.1 Chronaxie of TES model

Chronaxie values (T_{ch}) of the TES model were calculated from the simulated strength-duration curves depicted in Fig. 3 (Sect. 2.3). The calculated chronaxie values for the different nerve models are summarized in Table 2. The previously published chronaxie values that were obtained experimentally are shown in the same Table 2 and were determined for implantable systems where small electrodes were close to the nerve. For all nerve models the chronaxie values of the TES model were higher compared to the published chronaxie values. The chronaxie values using nerve models A, B, and D were in the range of experimentally obtained chronaxie values for TES, which are between 200 and 700 µs [15, 23, 48]. The largest increase was found in nerve model D, where the chronaxie
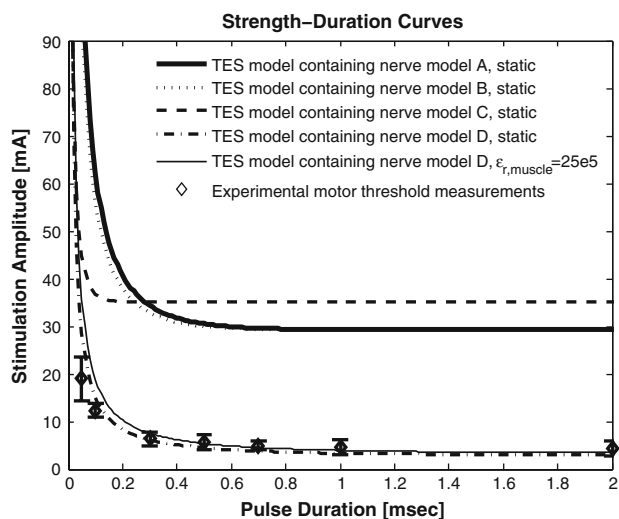
increased by 205% from 150 to 457 µs. The values with nerve model C (33 µs) were too short compared with the experimental range of 200–700 µs.

3.2 Influence of permittivities (capacitance)

The influence of the capacitive effects on Rec was investigated with the TES model using nerve model D. The permittivities (ε_r) of electrode, skin, fat, and muscle were changed in the range of published experimental values (Table 1). The results were produced for a stimulation pulse amplitude of 15 mA and a PD of 0.3 ms (values that are commonly applied on forearms using TES). Permittivity changes at the electrode-skin interface had no influence on Rec (<0.1%). Skin and fat permittivities changed Rec by 2%. The muscle permittivity had the largest influence with 5%. Strength-duration and recruitment-duration curves were therefore calculated for the published range of muscle permittivities (Table 1) in order to identify an upper limit for the influence of the capacitive effects.

Increasing the muscle permittivity shifted the strength-duration to slightly higher values (Fig. 3). The chronaxie was increased from 457 µs (static volume conductor) by 2% to 466 µs for $\varepsilon_r = 1.2e5$ and by 3.6% to 474 µs for $\varepsilon_r = 25e5$. These changes are small compared to the large variations of chronaxie values in experimental measurements of 200–700 µs [15, 23, 48].

The recruitment-duration curves for the smallest and largest muscle permittivity are depicted in Fig. 4. The
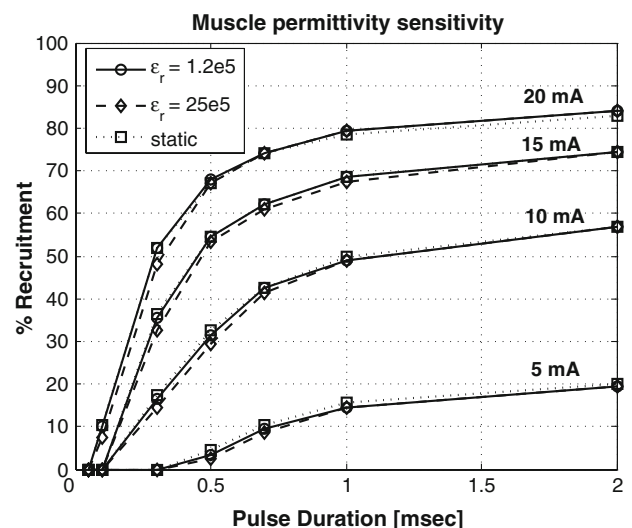

Fig. 3 Strength-duration curves from the TES model with the different tested nerve models (curve fit with Lapicque's equation). Additionally, the plot contains the experimentally obtained motor thresholds for different PDs (mean and standard deviation) measured in three human volunteers

Fig. 4 Recruitment-duration curves for different pulse amplitudes and the minimal and the maximal muscle permittivity (Table 1). Also shown are recruitment-duration curves calculated with a model using the static approximation of Eq. 1. The changes produced by the capacitance (permittivity) are seen to be small. (nerve model D was used)

curves show the percentage of axons that are activated in the nerve model for different pulse amplitudes and durations. The influence on the time constants τ_{sim} was largest for small pulse amplitudes. At 5 mA the time constant changed from 408 to 433 μs (6%) when increasing the permittivity from $1.2e5$ to $25e5$. However, the changes in recruitment due to the capacitive effects of the muscle are small compared to changes in recruitment caused by PD or pulse amplitude changes.

Figure 4 also shows the recruitment-duration curve described by a model that uses a static approximation (capacitive effects of the electrode-skin interface and the bulk tissues neglected) of Eq. 1 for the FE model. It can be seen that the curves are nearly congruent with the curves obtained using the model considering the permittivities.

3.3 Influence of tissue and stimulation parameters on chronaxie

The influence of different tissue and stimulation parameters on the chronaxie was investigated. Changing the tissue thicknesses and resistivities of the volume conductor model in the range of values that cover most human forearms (see Sect. 2.4) resulted in chronaxie changes below 1.1% for all four nerve models (percentage was calculated relative to the chronaxie values in Table 2). Only the thickest fat layer (30 mm) had a larger influence on the chronaxie (<6.3%). This is due to the spread of the current in the thicker fat layer that influences more nodes of the nerve models simultaneously (see Sect. 4).

Changes of electrode size and nerve depth have a larger influence on the chronaxie. The results using nerve model D are shown in Table 3 where it can be seen that the chronaxie values are in the range from 220 to 574 μs. In general, smaller electrodes and more superficial nerves result in smaller chronaxie values and vice versa. For nerve models A to C smaller electrodes and superficial nerves also generated smaller chronaxie values, however, the

Table 3 Simulated chronaxie values T_{ch} as observed in the results simulated by nerve model D (MRG) for different electrode sizes and two nerve depths (0.6 and 1.5 cm)

Electrode size (cm)	T_{ch} (0.6 cm) (μs)	T_{ch} (1.5 cm) (μs)
0.1	220	465
0.2	255	467
0.5	274	467
1	303	468
2	384	471
3	445	477
5	457	510
7	433	574

effect was less pronounced compared to nerve model D. The range of chronaxie values was 124–171 μs using nerve model A, 112–149 μs using nerve model B, and 27–36 μs using nerve model C.

3.4 Comparison of simulated with experimental strength-duration curves

The strength-duration curves that were calculated with the TES model containing the four tested nerve models (A–D) were compared with experimentally obtained motor threshold amplitudes (mean and standard deviation) for different PDs (see Fig. 3). The TES model with nerve model D matched best the experimental measurements for all measured PDs. The thresholds obtained with nerve models A, B, and C were all at least a factor of four higher. This was also indicated by the rheobasic currents (Table 2) that were too high for nerve models A, B, and C compared to the experiments.

3.5 Comparison of simulated with experimental recruitment-duration curves

The time constants τ_{sim} (Sect. 2.5) of the recruitment curves from the TES model were compared with the time constants τ_{exp} of the experimentally obtained recruitment curves. The TES models including nerve model A, B, or C used a current amplitude of 90 mA and the TES model with nerve model D used a current amplitude of 20 mA. The current amplitude for models A, B, and C had to be increased due to the higher rheobasic currents of these nerve models (Table 2).
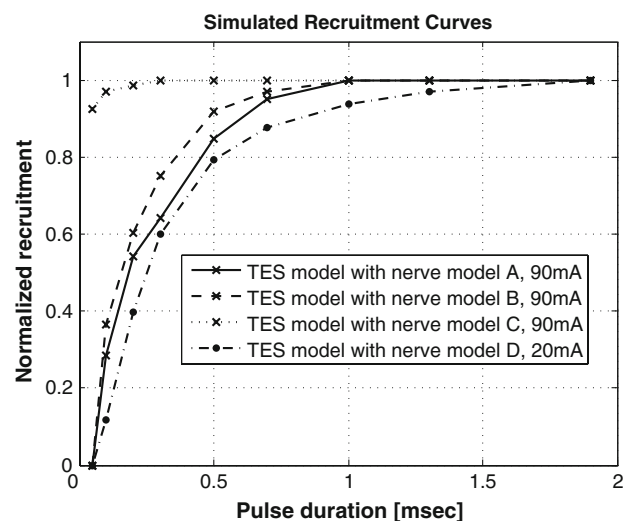

Fig. 5 Simulated recruitment-duration curves (normalized) using TES model with different nerve models (A–D)
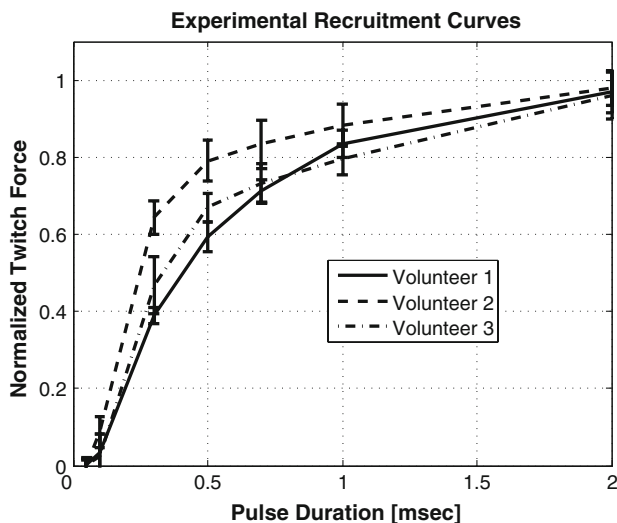
Experimental Recruitment Curves

Fig. 6 Recruitment-duration curves (normalized) of the middle finger from experimental measurements on three human volunteers. The stimulation amplitude was 20 mA

The normalized recruitment-duration curves obtained from simulations are shown in Fig. 5. The time constants τ_{sim} were 189 μs with nerve model A, 164 μs with nerve model B, 19 μs with nerve model C, and 476 μs with nerve model D. The experimentally measured recruitment curves from the upper extremities are shown in Fig. 6. The time constants τ_{exp} of these curves were 489 μs in volunteer one, 240 μs in volunteer two, and 380 μs in volunteer three. The time constants τ_{sim} obtained with the TES model containing nerve models A, B, or D were within the 95% confidence interval of the time constants τ_{exp} obtained by experimental measurements. The value of τ_{sim} derived from using nerve model C was more than a factor of ten shorter than the shortest τ_{exp}.

4 Discussion

We developed a two step model that describes the total dynamics from the applied stimulation current pulse to nerve recruitment for TES. The model enabled us to find out if published nerve models that were used in many studies for near-field stimulation with implantable electrodes are also suitable to describe far-field stimulation (TES). This was unclear because of the large discrepancy between the chronaxie values of published nerve models (30 and 150 μs) and chronaxie values obtained with surface electrodes (200 and 700 μs [15, 23, 48]). The simulation results in Table 2 show that the chronaxie values were increased when using the tested nerve models in the TES model. The chronaxie values were increased up to 205% compared with the chronaxie from publications, which were obtained with electrodes close to the axon. The

capacitive changes are not the reason for the increase as they had only a small influence (<6%). The results show that the electrode sizes and the electrode/nerve distance have the largest influence on chronaxie values amongst the tested parameters (Table 3). Smaller electrodes and smaller electrode/nerve distances resulted in smaller chronaxie values. This was also found in studies that investigated implantable electrodes close to the axon [44, 45]. Using different combinations of these two parameters in the TES model resulted in a range of 220–574 μs when using nerve model D that described best the published experimental range (200–700 μs) compared with the other tested nerve models (A–C). Possible reasons why nerve model D compared best with experiments are discussed in Sect. 4.1.

In order to find out how well the model describes TES, simulated strength-duration (Fig. 3) and recruitment-duration curves (Figs. 5 and 6) were compared with experimental measurements. The cylindrical geometry (tissue thicknesses), which we used (see Sect. 2) was specified such that it compared well to intermediate values of the three human volunteers (this was achieved using MRI scans in the same three human volunteers in an earlier study [27]). The results in Fig. 3 show that only the strength-duration curve using nerve model D (MRG-model) compared well with the experiments. The rheobasic currents using nerve models A, B, and C were too high. The recruitment-duration curves using nerve models A, B, and D compared well with experiments. The reason why not all nerve models compared well with experimental data can be partially explained due to different parameter values that were used in some nerve models (see Sect. 4.1). Until now the MRG-model was exclusively used for implanted ES systems [31]. With our investigations we could show that the MRG-model can also be used to model transcutaneous ES where the electrode/nerve distances are much larger than in implanted systems.

4.1 Parameter changes in used nerve models

It was investigated if changes in the parameters of nerve models A, B, and C can increase the chronaxie to values found with nerve model D. The parameters from nerve model D that mainly influence the chronaxie (membrane capacity, membrane resistivity, and axoplasm resistivity [44]) were applied to nerve models A, B, and C. The chronaxie values of nerve models A, B, and C were at the most increased by 20%. Therefore, most probably, the double cable structure, with explicit representation of the nodes of Ranvier, paranodal, and internodal sections [37] was responsible for the longer chronaxie and not the different parameters of nerve model D.

We showed that the TES models using nerve models A, B, or C had too high a rheobase (Sect. 3.4; Fig. 3). The

reason might be the different parameters of model D compared with models A, B, and C. The nodal leakage conductance g_L was 7 mS/cm^2 in D, but 30.3 mS/cm^2 in A and B, and 128 mS/cm^2 in C. The axoplasmatic resistivity ϱ_i was 70 Ωcm in D instead of 110 Ωcm in A and B, and 54.7 Ωcm in C. Applying the parameters from model D in model A and B lowered the thresholds at 0.2 ms PD from 36 to 10 mA in A and from 34 to 9 mA in B. These thresholds are closer to the experimentally obtained thresholds (see Fig. 3) of 6.3 mA. Applying the parameters from model D in model C did not significantly change the motor threshold found in the TES model containing nerve model C.

4.2 In which cases can the capacitive effects of the volume conductor be neglected?

The high variability of the electrode-skin interface and the published bulk tissue capacitances were found to have a minor influence on recruitment in TES (Fig. 4). Therefore, the capacitive effects can be neglected, which is equivalent to setting the time derivative term in Eq. 1 to zero yielding the Laplace equation. However, the capacitive effects of the volume conductor have to be considered in the model for the following cases:

– Investigations of time dependent voltage drops in the skin layer (which have a slow rise time): Such investigations are relevant if new pulse stimulation technologies, as for example presented in [19], are being developed. For such cases a model considering the capacitive effects allows one to optimize the power consumption because both the time dependent currents and the time dependent voltages can be simulated ($P(t) = U(t)*I(t)$).
– Investigation of voltage regulated stimulation: It is important to note that only a simulation that incorporates the tissues' capacitance is able to produce reasonable values for the extracellular potential at the axon for voltage regulated stimulation. The voltage drop in the skin layer increases over time because of the high skin capacitance [7] and thus the extracellular potential at the nerve significantly drops during the applied course of the pulse.

4.3 Spatial position of the nodes of ranvier

Axons with different diameters do not have the same internodal distance. As a consequence the nodes do not lie at the same position underneath the electrode and could lead to different activation thresholds. To investigate this we shifted the node of an axon by 0.1 mm steps within the internodal distance and could only observe

very small changes of the motor thresholds (<0.01 mA). The reason that the shifts did not have an influence was that the activation peaks were wider than the internodal distance.

4.4 Model limitations

The presented TES model has limitations that should be noted:

– In the presented TES model, nerve activation is calculated in two consecutive steps (FE model and nerve model). The coupling between the two steps is established by interpolating the potential field calculated using the FE model along the axons at $V_{e,n}(t)$ (extracellular potential). This interpolation is discrete in space and time which could introduce inaccuracies. The spatial interpolation is conducted at the axon models' nodes of Ranvier for axon models A–C. In nerve model D additionally an interpolation at the paranodal and the internodal sections was performed. To ensure a good accuracy of this interpolation the FE mesh size was refined until no significant change (<1%) was found in the resulting potential distribution. The temporal interpolation was performed in 1 μs steps, which is much shorter than the PD (>50 μs in our model), helping to ensure numerical accuracy.
– The two calculation steps of the TES model (FE model and nerve model) are performed in one direction. This means that the extracellular potential $V_{e,n}(t)$ affects the axons' TP, but the influence of the TP on the extracellular potential is neglected. Both directions were taken into account for the first time in [36] using a bidomain model. It was shown that the TP can influence the extracellular potential in direct muscle stimulation, however, it was not shown if the generation of APs in adjacent muscle fibers is significantly influenced. The method is computationally expensive and was therefore used on a simplified volume conductor which was coupled with two muscle fibers [36]. Since, the presented TES model contains a more detailed volume conductor and 1,000 axons, the solution could currently not be computed in reasonable time and remains an issue for future investigations.
– The non-linear dependence of the bulk tissue properties to current density was neglected. This is not a major concern as it was shown that with current-regulated pulses the non-linear properties of the bulk tissues can be neglected [28].
– Dispersion of the bulk tissues was neglected. Sensitivity studies [25] showed that a wide range of tissue properties did not influence neural activation. This indicates that dispersion can be neglected, too.

– The exact location where the APs are initiated in TES cannot be generalized due to geometrical and physiological diversity. We accounted for that by using multiple nerve bundles at different depths.

5 Conclusion

A FE model was combined with previously published active nerve models to a TES model. The TES model allows to describe the total dynamics from the applied stimulation current pulse to nerve recruitment and serves as a tool to investigate the influences from the geometry, the tissue properties, and new stimulation techniques.

For implantable stimulation (near-field) it was shown that mainly the electrode size and the electrode/nerve distance influence the chronaxie. Our results show that the chronaxie is also in the far-field situation mainly influenced by the electrode size and the electrode/nerve distance. With electrode sizes between (0.1 and 7 cm) and electrode/axon distances between 0.6 and 1.5 cm chronaxie values between 220 and 574 μs were obtained. The capacitive effects, variations of the tissue resistivities, and variations of the tissue thicknesses have a minor influence.

Simulated strength-duration and recruitment-duration curves using the MRG-nerve-model (model D) compared well with experimental measurements. We conclude from these results that the MRG-model can be used with the same parameters for both implantable ES models and TES models. The parameters of the other tested nerve models have to be adapted to compare well with experimental measurements.

With the presented TES model we developed a tool that should help to investigate and optimize new TES technologies, such as multi-channel electrode arrays using non-uniform current distributions. It should help to find appropriate designs for electrode geometries and stimulation pulse sequences.

References

1. Bajzek TJ, Jaeger RJ (1987) Characterization and control of muscle response to electrical stimulation. Ann Biomed Eng 15:485–501
2. Baker LL, McNeal DR, Benton L, Bowman BR, Waters RL (2000) Neuro muscular electrical stimulation, 4th edn
3. Bostock H (1983) The strength-duration relationship for excitation of myelinated nerve: computed dependence on membrane parameters. J Physiol 341:59–74
4. Chiu SY, Ritchie JM, Rogart RB, Stagg D (1979) A quantitative description of membrane currents in rabbit myelinated nerve. J Physiol 292:149–166
5. Chou LW, Binder-Macleod SA (2007) The effects of stimulation frequency and fatigue on the force-intensity relationship for human skeletal muscle. Clin Neurophysiol 118:1387–1396
6. Crago PE, Peckham PH, Mortimer JT, Van der Meulen JP (1974) The choice of pulse duration for chronic electrical stimulation via surface, nerve, and intramuscular electrodes. Ann Biomed Eng 2:252–264
7. Dorgan SJ, Reilly RB (1999) A model for human skin impedance during surface functional neuromuscular stimulation. IEEE Trans Rehabil Eng 7:341–348
8. Elsaify A, Fothergill J, Peasgood W (2004) A portable fes system incorporating an electrode array and feedback sensors. In: Vienna Int. Workshop on Functional Electrostimulation, vol 8, pp 191–194
9. Fitzhugh R (1962) Computation of impulse initiation and saltatory conduction in a myelinated nerve fiber. Biophys J 2:11–21
10. Foster KR, Schwan HP (1989) Dielectric properties of tissues and biological materials: a critical review. Crit Rev Biomed Eng 17:25–104
11. Frankenhaeuser B, Huxley AF (1964) The action potential in the myelinated nerve fiber of xenopus laevis as computed on the basis of voltage clamp data. J Physiol 171:302–315
12. Gabriel S, Lau RW, Gabriel C (1996) The dielectric properties of biological tissues: Iii. parametric models for the dielectric spectrum of tissues. Phys Med Biol 41:2271–2293
13. Geddes LA (2004) Accuracy limitations of chronaxie values. IEEE Trans Biomed Eng 51:176–181
14. Gregory CM, Dixon W, Bickel CS (2007) Impact of varying pulse frequency and duration on muscle torque production and fatigue. Muscle Nerve 35:504–509
15. Harris R (1971) Chronaxy. In: SL (ed) Electrodiagnosis and electromyography, Baltimore, pp 218–239
16. Hines ML, Carnevale NT (2001) Neuron: a tool for neuroscientists. Neuroscientist 7:123–135
17. Hodgkin AL, Huxley AF (1952) A quantitative description of membrane current and its application to conduction and excitation in nerve. J Physiol 117:500–544
18. Holsheimer J, Wesselink WA (1997) Optimum electrode geometry for spinal cord stimulation: the narrow bipole and tripole. Med Biol Eng Comput 35:493–497
19. Jezernik S, Morari M (2005) Energy-optimal electrical excitation of nerve fibers. IEEE Trans Biomed Eng 52:740–743
20. Keller T, Popovic M, Amman M, Andereggen C, Dumont C (2000) A system for measuring finger forces during grasping. In: International functional electrical stimulation society conference, Aalborg, Denmark
21. Keller T, Popovic MR, Pappas IPI, Muller PY (2002) Transcutaneous functional electrical stimulator "compex motion". Artif Organs 26:219–223
22. Kesar T, Binder-Macleod S (2006) Effect of frequency and pulse duration on human muscle fatigue during repetitive electrical stimulation. Exp Physiol 91:967–976
23. Kiernan MC, Burke D, Andersen KV, Bostock H (2000) Multiple measures of axonal excitability: a new approach in clinical testing. Muscle Nerve 23:399–409
24. Kuhn A, Keller T (2005) A 3d transient model for transcutaneous functional electrical stimulation. In: International functional electrical stimulation society conference, vol 10, Montreal, Canada, pp 385–387
25. Kuhn A, Keller T (2006) The influence of capacitive properties on nerve activation in transcutaneous electrical stimulation. In: International symposium on computer methods in biomechanics and biomedical engineering, vol 7, Antibes, France

26. Kuhn A, Rauch GA, Keller T, Morari M, Dietz V (2005) A finite element model study to find the major anatomical influences on transcutaneous electrical stimulation. In: ZNZ Symposium, Zurich, Switzerland

27. Kuhn A, Rauch GA, Panchaphongsaphak P, Keller T (2005) Using transient fe models to assess anatomical influences on electrical stimulation. In: FEM Workshop, vol 12, Ulm, Germany

28. Kuhn A, Keller T, Prenaj B, Morari M (2006) The relevance of non-linear skin properties for a transcutaneous electrical stimulation model. In: International functional electrical stimulation society conference, vol 11, Zao, Japan

29. Lapicque L (1907) Recherches quantitatives sur l'excitation electrique des nerfs traitee comme une polarisation. J Physiol Paris 9:622–635

30. Lawrence M, Pitschen G, Keller T, Kuhn A, Morari M (2008) Finger and wrist torque measurement system for the evaluation of grasp performance with neuroprosthesis. Artif Organs (in press)

31. Lertmanorat Z, Gustafson KJ, Durand DM (2006) Electrode array for reversing the recruitment order of peripheral nerve stimulation: experimental studies. Ann Biomed Eng 34:152–160

32. Livshitz LM, Einziger PD, Mizrahi J (2002) Rigorous green's function formulation for transmembrane potential induced along a 3-d infinite cylindrical cell. IEEE Trans Biomed Eng 49:1491–1503

33. Manola L, Roelofsen BH, Holsheimer J, Marani E, Geelen J (2005) Modelling motor cortex stimulation for chronic pain control: electrical potential field, activating functions and responses of simple nerve fibre models. Med Biol Eng Comput 43:335–343

34. Martinek J, Reichel M, Rattay F, Mayr W (2004) Analysis of calculated electrical activation of denervated muscle fibres in the human thigh. In: Proceedings of 8th Vienna international workshop on functional electrical stimulation, pp 228–231

35. Martinek J, Stickler Y, Dohnal F, Reichel M, Mayr W, Rattay F (2006) Simulation der funktionellen elektrostimulation im menschlichen oberschenkel unter verwendung von femlab. In: Proceedings of the COMSOL Users Conference 2006, Frankfurt, pp 20–23

36. Martinek J, Stickler Y, Reichel M, Rattay F (2007) A new approach to simulate hodgkin-huxley like excitation with comsol multiphysics (femlab). In: Proceedings of 9th Vienna international workshop on functional electrical stimulation, pp 163–166

37. McIntyre CC, Richardson AG, Grill WM (2002) Modeling the excitability of mammalian nerve fibers: influence of afterpotentials on the recovery cycle. J Neurophysiol 87:995–1006

38. McNeal DR (1976) Analysis of a model for excitation of myelinated nerve. IEEE Trans Biomed Eng 23:329–337

39. Mesin L, Merletti R (2008) Distribution of electrical stimulation current in a planar multilayer anisotropic tissue. IEEE Trans Biomed Eng 55:660–670

40. Polk C (1986) CRC handbook of biological effects of electromagnetic fields. CRC Press, Boca Raton

41. Prodanov D, Feirabend HK (2007) Morphometric analysis of the fiber populations of the rat sciatic nerve, its spinal roots, and its major branches. J Comp Neurol 503:85–100

42. Rattay F (1990) Electrical nerve stimulation theory, experiments and applications. Springer, Wien

43. Reichel M, Martinek J, Mayr W, Rattay F (2004) Functional electrical stimulation of denervated skeletal muscle fibers in 3d human thigh—modeling and simulation. In: Proceedings of 8th Vienna international workshop on functional electrical stimulation, pp 44–47

44. Reilly JP, Bauer RH (1987) Application of a neuroelectric model to electrocutaneous sensory sensitivity: parameter variation study. IEEE Trans Biomed Eng 34:752–754

45. Reilly JP, Antoni H, Chilbert MA, Sweeney JD (1998) Applied bioelectricity from electrical stimulation to electropathology. Springer, New York

46. Rijkhoff NJ, Holsheimer J, Koldewijn EL, Struijk JJ, van Kerrebroeck PE, Debruyne FM, Wijkstra H (1994) Selective stimulation of sacral nerve roots for bladder control: a study by computer modeling. IEEE Trans Biomed Eng 41:413–24

47. Schiefer MA, Triolo RJ, Tyler DJ (2008) A model of selective activation of the femoral nerve with a flat interface nerve electrode for a lower extremity neuroprosthesis. IEEE Trans Neural Syst Rehabil Eng 16:195–204

48. Schuhfried O, Kollmann C, Paternostro-Sluga T (2005) Excitability of chronic hemiparetic muscles: determination of chronaxie values and strength-duration curves and its implication in functional electrical stimulation. IEEE Trans Neural Syst Rehabil Eng 13:105–109

49. Sotiropoulos SN, Steinmetz PN (2007) Assessing the direct effects of deep brain stimulation using embedded axon models. J Neural Eng 4:107–119

50. Standring S (2005) Gray's Anatomy, 39th edn

51. Strickler Y, Martinek J, Hofer C, Rattay F (2007) A finite element model of the electrically stimulated human thigh: Changes due to denervation and training. In: Proc. of 9th Vienna International Workshop on Functional Electrical Stimulation, Krems, Austria, pp 20–23

52. Sweeney J, Mortimer J, Durand D (1987) Modeling of mammalian myelinated nerve for functional neuromuscular stimulation. In: Proc. of IEEE 9th Annual Conference of the Engineering in Medicine and Biology Society, pp 1577–1578

53. Valentin J (2001) Basic anatomical and physiological data for use in radiological protection: reference values. Ann ICRP

54. Vodovnik L, Crochetiere WJ, Reswick JB (1967) Control of a skeletal joint by electrical stimulation of antagonists. Med Biol Eng 5:97–109

55. Zierhofer CM (2001) Analysis of a linear model for electrical stimulation of axons–critical remarks on the "activating function concept". IEEE Trans Biomed Eng 48:173–184